

The Mass of the Black Hole in the Quasar PG 2130+099

C. J. Grier¹, B. M. Peterson^{1,2}, M. C. Bentz³, K. D. Denney¹, J. D. Eastman¹,
M. Dietrich¹, R. W. Pogge^{1,2}, J. L. Prieto¹, D. L. DePoy^{1,2}, R. J. Assef¹, D. W. Atlee¹,
J. Bird¹, M. E. Eyler⁴, M. S. Peeples¹, R. Siverd¹, L. C. Watson¹, J. C. Yee¹

ABSTRACT

We present the results of a recent reverberation-mapping campaign undertaken to improve measurements of the radius of the broad line region and the central black hole mass of the quasar PG 2130+099. Cross correlation of the 5100 Å continuum and H β emission-line light curves yields a time lag of $22.9^{+4.4}_{-4.3}$ days, corresponding to a central black hole mass $M_{\text{BH}} = (3.8 \pm 1.5) \times 10^7 M_{\odot}$. This value supports the notion that previous measurements yielded an incorrect lag. We re-analyzed previous datasets to investigate the possible sources of the discrepancy and conclude that previous measurement errors were apparently caused by a combination of undersampling of the light curves and long-term secular changes in the H β emission-line equivalent width. With our new measurements, PG 2130+099 is no longer an outlier in either the $R_{\text{BLR}}-L$ or the $M_{\text{BH}}-\sigma_*$ relationships.

Subject headings: galaxies: active — galaxies: nuclei — galaxies: Seyfert — quasars: emission lines

1. INTRODUCTION

Reverberation mapping uses observations of continuum and emission-line variability to probe the structure of the broad line region (BLR) in active galactic nuclei (Blandford & McKee 1982; Peterson 1993). It has been extensively used to estimate the physical size of

¹Department of Astronomy, The Ohio State University, 140 W 18th Ave, Columbus, OH 43210

²Center for Cosmology & AstroParticle Physics, The Ohio State University, 191 West Woodruff Ave, Columbus, OH 4321

³Department of Physics and Astronomy, University of California at Irvine, 4129 Frederick Reines Hall, Irvine, CA 92697

⁴Department of Physics, U.S. Naval Academy, 572C Holloway Road, Annapolis, MD 21401

the BLR and the mass of central black holes in active galactic nuclei (AGN). The observed continuum variability precedes the observed emission-line variability by a time related to the light travel time across the BLR; by obtaining an estimate of the time delay, or “lag” τ , between the change in continuum flux and the change in emission-line flux, one can estimate the size of the BLR. While this is an extremely effective method, high-quality datasets are difficult to obtain, as they require well-spaced observations over long timescales. To date, over three dozen AGN have estimated black hole masses obtained using reverberation methods.

In addition to being important physical parameters, the BLR radius and central black hole mass (M_{BH}) measurements are crucial in calibrating relationships between different properties of AGN. A useful relationship that has emerged is the correlation between the radius of the BLR (R_{BLR}) and the optical luminosity of the AGN (e.g. Kaspi et al. 2000, 2005; Bentz et al. 2006). Another key relationship is that between M_{BH} and bulge stellar velocity dispersion (σ_*) which is seen in both quiescent (Ferrarese & Merritt 2000; Gebhardt et al. 2000a; Tremaine et al. 2002) and active galaxies (Gebhardt et al. 2000b; Ferrarese et al. 2001; Nelson et al. 2004; Onken et al. 2004; Dasyra et al. 2007). These two relationships are critical because they allow us to estimate the masses of black holes in AGN from a single spectrum (see McGill et al. 2008 for a recent summary) — we estimate R_{BLR} from the AGN luminosity, the velocity dispersion of the BLR is determined by the emission-line width, and the quiescent $M_{\text{BH}}-\sigma_*$ relationship provides the calibration of the reverberation-based mass scale. Obtaining high-quality single-epoch spectra is much less observationally demanding than obtaining high-quality reverberation measurements; once relations such as these are properly calibrated, we can measure M_{BH} in many more objects than would otherwise be possible. An extensive set of objects with reliable black hole masses allows us to explore the connection between black holes and AGN evolution over cosmologically interesting timescales.

PG 2130+099 has been a source of curiosity because it is an outlier in both the $M_{\text{BH}}-\sigma_*$ and $R_{\text{BLR}}-L$ relations. Previous measurements obtained by Kaspi et al. (2000) and reanalyzed by Peterson et al. (2004) found $\text{H}\beta$ lags of about 180 days. These measurements yield a black hole mass M_{BH} upwards of $10^8 M_{\odot}$. At luminosity $\lambda L_{\lambda}(5100 \text{ \AA})=(2.24 \pm 0.27) \times 10^{44} \text{ erg s}^{-1}$, this places PG 2130+099 well above the $R_{\text{BLR}}-L$ relationship (Bentz et al. 2006). Dasyra et al. (2007) also note that PG 2130+099 falls above the $M_{\text{BH}}-\sigma_*$ relationship. Together these suggest that this discrepancy could be caused by measurement errors in the BLR radius. Our suspicions are also fueled by two other factors. First, the optical spectrum of PG 2130+099 is similar to that of narrow-line Seyfert 1 (NLS1) galaxies, which are widely supposed to be AGN with high accretion rates relative to the Eddington rate (see Komossa 2008 for a recent review). However, the accretion rate derived from this mass and luminosity

(under common assumptions for all reverberation-mapped AGN as described by Collin et al. 2006) is quite low compared to NLS1s, again suggesting that M_{BH} and therefore τ are overestimated. Second, as we discuss further below, a lag of approximately half a year on an equatorial source means that fine-scale structure in the two light curves will not match up in detail, and cross-correlation becomes very sensitive to long-term secular variations that may or may not be an actual reverberation signal.

For these reasons, we decided to undertake a new reverberation campaign to remeasure the $\text{H}\beta$ lag for PG 2130+099. In this paper, we present a new lag determination from this campaign. We also present a re-analysis of the earlier dataset that suggests that the true lag is consistent with our new lag value and investigate possible sources of error in the previous analysis.

2. OBSERVATIONS AND DATA ANALYSIS

2.1. Observations

The data were obtained as a part of queue-scheduled program during the SDSS-II Supernova Survey follow-up campaign (Frieman et al. 2008). We obtained spectra of PG 2130+099 with the Boller and Chivens CCD Spectrograph on the MDM 2.4m telescope for 21 different nights from 2007 September through 2007 December. We used a 150 grooves/mm grating which yields a dispersion of $3.29 \text{ \AA pixel}^{-1}$ and covers the spectral range 4000–7500 \AA . The slit width was set to $3''.0$ projected on the sky and the spectral resolution was 15.2 \AA . We used an extraction aperture that corresponds to $3''.0 \times 7''.0$.

2.2. Light Curves

The reduced spectra were flux-calibrated using the flux of the $[\text{O III}] \lambda 5007$ emission line in a reference spectrum created using a selection of 9 nights with the best observing conditions. Using a χ^2 goodness-of-fit estimator method (van Groningen & Wanders 1992), each individual spectrum was scaled to the reference spectrum. For three epochs, no reasonable fit could be obtained, hence we scaled these spectra by hand to match the $[\text{O III}] \lambda 5007$ flux of the reference spectrum, which was $1.36 \times 10^{-13} \text{ erg s}^{-1} \text{ cm}^{-2}$ in the observed frame ($z = 0.06298$). We then removed the narrow-line components of the $\text{H}\beta$ and $[\text{O III}] \lambda\lambda 4959, 5007$ lines using relative line strengths given by Peterson et al. (2004). Figure 1 shows the mean and rms spectra of PG 2130+099, created from the entire set of 21 flux-calibrated observations.

To measure the continuum and line fluxes, we fit a line to the continuum between the regions 5050–5070 Å and 5405–5435 Å in the observed frame. We measured the H β flux by integrating the flux above the continuum from 5070–5285 Å, and the optical continuum flux was taken to be the average flux in the range 5405–5435 Å. Errors were estimated based on differences between observations that were close together in time. The observations from 2007 September 27 (JD 2454371) had an extremely low signal-to-noise ratio (S/N) compared to the rest of the population; following Peterson et al. (1998a), we assigned fractional errors of $1/(S/N)$ for this night in both the continuum and line flux. The resulting continuum and H β light curves are given in Table 1 and are shown in Figure 2. The properties of the final light curves used in our time series analysis are given in Table 2. Column (1) gives the spectral feature and Column (2) gives the number of points in the individual light curves. Columns (3) and (4) give the average and median time spacing between observations, respectively. Column (5) gives the mean flux of the feature in the observed frame, and Column (6) gives the mean fractional error that is computed based on observations that are closely spaced. Column (7) gives the excess variance, defined by

$$F_{\text{var}} = \frac{\sqrt{\sigma^2 - \delta^2}}{\langle f \rangle} \quad (1)$$

where σ^2 is the flux variance of the observations, δ^2 is the mean square uncertainty, and $\langle f \rangle$ is the mean observed flux. Column (8) is the ratio of the maximum to minimum flux in each light curve.

We note in passing that we attempted to determine light curves for the other prominent emission lines in our spectra, H α and H γ . Unfortunately, the fidelity of our flux calibration decreases away from the [O III] λ 5007 line (which we believe accounts for the increasing strength of the rms spectrum longward of ~ 5800 Å in Figure 1) and, combined with the low amplitude of variability, renders the other light curves unreliable. Nevertheless, time series analysis yields results that are at least consistent with the H β results, though with much larger uncertainties.

3. TIME SERIES ANALYSIS

3.1. Time delay measurements

To measure the lag between the optical continuum and H β emission-line variations, we cross-correlated the H β light curve with the continuum light curve using the interpolation method originally described by Gaskell & Sparke (1986) and Gaskell & Peterson (1987) and subsequently modified by White & Peterson (1994) and Peterson et al. (1998b, 2004). The

method works as follows: because the data are not evenly spaced in time, we interpolate between points to obtain an evenly-sampled light curve. The linear correlation coefficient r is then calculated using pairs of points, one from each light curve, separated by a given time lag. When r is calculated for a range of time lag values, the cross correlation function (CCF) is obtained, which consists of the value of r for each time lag value. We interpolated between the points on a 0.5 day timescale to obtain the CCF for our dataset, which is shown in Figure 3.

To determine the most probable delay and its uncertainty, we employed the flux randomization/random subset sampling Monte Carlo method described by Peterson et al. (1998b). The “random subset sampling” method takes a light curve of N points and samples it N times without regard to whether or not any given point has been selected already. The flux uncertainty of a data point selected n times is correspondingly reduced by a factor $n^{-1/2}$ (Welsh 1999; Peterson et al. 2004). The flux value of each point is then altered by a random Gaussian deviate based on the uncertainty assigned to the point; this is known as “flux randomization”. A CCF was calculated for each altered light curve using interpolation as before. Using 2000 iterations of this process, we obtain a distribution of τ_{peak} , measured from the CCF of each Monte Carlo realization and defined by the location of the peak value of r . We also calculate and obtain a distribution of the lag values τ_{cent} that represents the centroid of each CCF using the points surrounding the peak, based on all lag values with $r \geq 0.8r_{\text{max}}$. We then adopt the mean values of both the centroid and peak $\langle \tau_{\text{cent}} \rangle$ and $\langle \tau_{\text{peak}} \rangle$ for our analysis. We estimate the uncertainties in τ_{cent} and τ_{peak} such that 15.87% of the realizations fall below the mean minus the lower error and 15.87% of the realizations fall above the mean plus the upper error. Our final lag values and errors are $\tau_{\text{cent}} = 22.9^{+4.4}_{-4.3}$ days and $\tau_{\text{peak}} = 22.2^{+5.6}_{-5.2}$ days in the rest frame of PG 2130+099. It is important to note that the CCF is heavily dependent on the timespan of the light curve relative to the actual delay, and if the data timespan is short with respect to the lag, the CCF will be biased towards short lag measurements (Welsh 1999). We note that because our data span just over three months, our CCF is not capable of producing a lag measurement as large as previous measurements and is subject to this bias. However, if the actual lag is shorter as the evidence presented in this work suggests, our data span a sufficiently long period to identify the true delay.

As a check on our time series analysis, we also employed an alternative method known as the z -transformed discrete correlation function (ZDCF), as described by Alexander (1997). This method is a modification of the discrete correlation function (DCF) described by Edelson & Krolik (1988). The DCF is obtained by correlating data points from the continuum with points from the $H\beta$ light curve by binning the data in time rather than interpolating between points. The ZDCF similarly uses bins rather than interpolation, but bins the data by equal population rather than by equal spacing in time and applies Fisher’s z -transform

to the cross correlation coefficients. Discrete correlation functions have the advantage that they only use real data points, and are therefore less likely to find spurious correlations in data where there are large time gaps. However, datasets with few points tend to yield lag values with large uncertainties; hence this method is primarily useful as a check on the interpolation method when the data are undersampled. Figure 3 shows the computed ZDCF for our PG 2130+099 dataset. It should be noted that the z -transform requires a minimum of 11 points per bin to be statistically significant (Alexander 1997); because our light curves contained only 21 points, we were unable to obtain a well-sampled ZDCF with a minimum of 11 points per bin. We used a minimum of 8 points per bin and do not obtain an independent lag measurement, but the ZDCF is very consistent with our calculated CCF, indicating that the interpolation results are credible.

3.2. Line width measurement and mass calculations

We use the second moment of the line profile, σ_{line} (Fromerth & Melia 2000; Peterson et al. 2004) to characterize the width of the $H\beta$ line. To determine the best value of σ_{line} and its uncertainties, we use Monte Carlo simulations similar to those used in determining the time lag (see Peterson et al. 2004). We measure the line widths from both the mean and rms spectra created in the simulations from N randomly chosen spectra and correct them for the spectrograph resolution. We obtain a distribution of each line width from multiple realizations, from which we take the mean value for our measure of σ_{line} or FWHM and the standard deviation as the measurement uncertainty. The measured line widths and uncertainties are given in Table 3.

Assuming that the motion of the $H\beta$ -emitting gas is dominated by gravity, the relation between M_{BH} , line width, and time delay is

$$M_{\text{BH}} = \frac{fc\tau\Delta V^2}{G}, \quad (2)$$

where τ is the emission-line time delay, ΔV is the emission-line width, and f is a dimensionless factor that is characterized by the geometry and kinematics of the BLR. Onken et al. (2004) calculated an average value of $\langle f \rangle$ by assuming that AGN follow the same $M_{\text{BH}}-\sigma_*$ relationship as quiescent galaxies. By normalizing the reverberation black hole masses to the relation for quiescent galaxies, they obtain $\langle f \rangle = 5.5$ when the line width is characterized by the line dispersion σ_{line} of the rms spectrum.¹ Using our values of τ_{cent} and σ_{line} , we compute

¹Differences between the use of σ_{line} and the FWHM in calculating M_{BH} are discussed by Collin et al. (2006).

$$M_{\text{BH}} = (3.8 \pm 1.5) \times 10^7 M_{\odot}.$$

We also compute the average 5100 Å luminosity of our sample to see where our new R_{BLR} value places PG 2130+099 on the $R_{\text{BLR}}-L$ relationship. Following Bentz et al. (2006), we correct our luminosity for host-galaxy contamination. Assuming $H_0 = 70 \text{ km s}^{-1} \text{ Mpc}^{-1}$, $\Omega_{\text{m}} = 0.30$ and $\Omega_{\Lambda} = 0.70$, we calculate $\log \lambda L_{\lambda}(5100 \text{ Å}) = 44.40 \pm 0.02$ for our recent measurements of PG 2130+099. The relevant measurements and computed quantities are given in Table 4.

4. DISCUSSION

Analysis of previous datasets of PG 2130+099 yields lags greater than 150 days and M_{BH} values above $10^8 M_{\odot}$, in both cases approximately an order of magnitude larger than our new value. To investigate the source of these discrepancies, we closely scrutinized the previous dataset, which consists of data obtained at Steward Observatory and Wise Observatory (Kaspi et al. 2000). The 5100 Å continuum and emission-line light curves, along with their respective CCF and ZDCFs, are shown in Figure 4. We first ran the full light curve through the time series analysis as described in section 2.3 to confirm the previous results, and successfully reproduced a lag measurement of ~ 168 days, in agreement with Kaspi et al. (2000) and Peterson et al. (2004). However, visual inspection of the light curves suggests that these values were in error; we were able to identify several features that are present in the continuum, H β and H α light curves that are quite visibly lagging on timescales shorter than 50 days, as we show below.

It is clear that the Kaspi et al. results are dominated by the data spanning the years 1993-1995, as this period contains the most significant variability as well as time sampling that is sufficient to resolve features in the light curves. We show the light curves for all spectral features measured by Kaspi et al. during this time period in Figure 5. Over this period, we can match behavior in the continuum with the behavior of the emission lines, most noticeably in the data from 1995. The most prominent features in the light curves are the maximum in the continuum at the end of the 1994 series and the maxima in the lines at the beginning of the 1995 series, which, based on the continuum variations, one would expect to be lower relative to the fluxes in 1994. However, inspection of the relative flux levels of the lines and continuum in the 1994 and 1995 data reveals that the equivalent width of the emission lines changes during this timespan, which results in a rise in emission-line flux apparently unrelated to reverberation. The maximum in the continuum and those in the emission lines do not correspond to the same features— the maxima in the emission line light curves in 1995 correspond to the similar feature in the continuum at the beginning of

1995. Because there are no observations during the six months or so between these features, the CCF and ZDCF lock onto the two unrelated maxima that are separated by 196 days and yield lags of ~ 200 days over this three-year span. The emission lines likely continued to increase in flux during the time period for which there were no observations.

Inspection of the light curve segments in Figure 5 reveals similar structures in each of them within a given year. To quantify the time delays between the continuum and lines on short timescales, we cross-correlated each individual year, this time using only flux randomization in the Monte Carlo realizations, as there were too few points in each year to use random subset sampling, so the uncertainties are underestimated. The resulting lags are given in Table 5. Again we must consider that the CCF cannot produce a lag that is greater than the duration of observations, so the individual CCFs for these three years are limited to short delays. However, the presence of the 1995 feature in both the continuum and emission-line light curves is unmistakable and it is extremely unlikely that it lags by a value exceeding the sensitivity limit of the CCF. From this we surmise that the discrepancies in measured lag values are mostly a result of large time gaps in the data and/or underestimation of the error bars in the Kaspi et al. data.

Welsh (1999), and even earlier, Pérez, Robinson, & de la Fuente (1992), pointed out that emission-line lags can be severely underestimated with light curves that are too short in duration, particularly if the BLR is extended: certainly our 98-day campaign is insensitive to lags as long as ~ 180 days. Is it possible that the original lag determination of Kaspi et al. (2000) and Peterson et al. (2004) is correct (or more nearly so) and we have been fooled by reliance on light curves that are too short? We think not, based on (1) the reasonable match between details in the continuum and emission-line light curves for four different observing seasons (1993, 1994, 1995, and 2007), (2) the improved agreement with the $R_{\text{BLR}}-L$ relationship with the smaller lag (demonstrated in Figure 6), and (3) the improved agreement with the $M_{\text{BH}}-\sigma_*$ relationship with the smaller lag (Figure 7). It is also worth pointing out the difficulty of accurately measuring a ~ 180 day lag, particularly in the case of equatorial sources which have a relatively short observing season. The short observing season, typically 6-7 months, means that there are very few emission-line observations that can be matched directly with continuum points: the observed emission-line fluxes represent a response to continuum variations that occurred when the AGN was too close to the Sun to observe.

Welsh (1999) has also pointed out the value in “detrending” the light curves—removing long-term trends by fitting the light curves with a low-order function can reduce the bias toward underestimating lags. In this particular case, we find that detrending has almost no effect: in particular, the highest points in the continuum (in late 1994) and the highest

points in the line (early in the 1995 observing season) remain so after detrending, and both the interpolation CCF and ZDCF weight these points heavily. It is also interesting to note that the peak in the ZDCF agrees with the peak of the interpolation CCF (Figure 4), which demonstrates that the ~ 180 day lag is *not* simply ascribable to interpolation across the gap between the 1994 and 1995 observing seasons.

The data from our 2007 campaign are not ideal: the amplitude of variability was low, the time sampling was adequate, but only barely, and the duration of the campaign was short enough that we lack sensitivity to lags of ~ 50 days or longer. But the preponderance of evidence at this point argues that our smaller lag measurement is more likely to be correct than the previous determination. Certainly better-sampled light curves of longer duration would yield a more definitive result.

5. SUMMARY

From a new reverberation campaign, we obtain a measurement of the time lag of the $H\beta$ line in PG 2130+099 of $\tau_{\text{cent}} = 22.9^{+4.4}_{-4.3}$ days and calculate a central black hole mass $M_{\text{BH}} = (3.8 \pm 1.5) \times 10^7 M_{\odot}$. Previous measurements of τ_{cent} overestimated the size of the BLR and therefore the mass of the black hole, most likely due to the undersampling in the light curves. A re-analysis of the previous data, using both visual and algorithmic methods, suggests that the true BLR size and M_{BH} are consistent with our new values. The recent reverberation measurements for PG 2130+099 presented in this study remove the discrepancies previously found for this object based on the $M_{\text{BH}}-\sigma_*$ and $R_{\text{BLR}}-L$ relationships.

We are grateful for support of this program by the National Science Foundation through grant AST-0604066 to The Ohio State University. We would also like to thank H. Netzer, S. Kaspi, and referee C. M. Gaskell for their helpful suggestions.

REFERENCES

- Alexander, T. 1997, in *Astronomical Time Series*, ed. D. Maoz, A. Sternberg, & E.M. Leibowitz (Dordrecht: Kluwer), 163
- Bentz, M.C., Peterson, B.M., Pogge, R.W., Vestergaard, M., & Onken, C.A. 2006, *ApJ*, 644, 133

- Bentz, M.C., Peterson, B.M., Netzer, H., Pogge, R.W., & Vestergaard, M. 2008, *ApJ*, submitted
- Blandford, R.D., & McKee, C.F. 1982, *ApJ*, 255, 419
- Collin, S., Kawaguchi, T., Peterson, B.M., & Vestergaard, M. 2006, *A&A*, 456, 75
- Dasyra, K.M., Tacconi, L.J., Davies, R.I., Genzel, R., Lutz, D., Peterson, B.M., Veilleux, S., Baker, A.J., Schweitzer, M., & Sturm, E. 2007, *ApJ*, 657, 102
- Edelson, R.A., & Krolik, J.H. 1988, *ApJ*, 333, 646
- Ferrarese, L., & Merritt, D.M. 2000, *ApJ*, 539, L9
- Ferrarese, L., Pogge, R.W., Peterson, B.M., Merritt, D., Wandel, A., & Joseph, C.L. 2001, *ApJ*, 555, L79
- Frieman, J. A., et al. 2008, *AJ*, 135, 338
- Fromerth, M.J., & Melia, F. 2000, *ApJ*, 533, 172
- Gaskell, C.M., & Peterson, B.M. 1987, *ApJS*, 65, 1
- Gaskell, C.M., & Sparke, L.S. 1986, *ApJ*, 305, 175
- Gebhardt, K., et al. 2000a, *ApJ*, 539, L13
- Gebhardt, K., et al. 2000b, *ApJ*, 543, L5
- Kaspi, S., Maoz, D., Netzer, H., Peterson, B.M., Vestergaard, M., & Jannuzi, B.T. 2005, *ApJ*, 629, 61
- Kaspi, S., Smith, P.S., Netzer, H., Maoz, D., Jannuzi, B.T., & Giveon, U. 2000, *ApJ*, 533, 631
- Komossa, S. 2008, in *The Nuclear Region, Host Galaxy, and Environment of Active Galaxies*, ed. E. Benítez, I. Cruz-González, and Y. Krongold, *Revista Mexicana de Astronomía y Astrofísica (Serie de Conferencias)*, Vol. 32, pp. 86-92
- McGill, K.L., Woo, J.-H., Treu, T., Malkan, M.A. 2008, *ApJ*, 673, 703
- Nelson, C.H., Green, R.F., Bower, G., Gebhardt, K., & Weistrop, D. 2004, *ApJ*, 615, 652
- Onken, C.A., Ferrarese, L., Merritt, D., Peterson, B.M., Pogge, R.W., Vestergaard, M., & Wandel, A. 2004, *ApJ*, 615, 645

Peterson, B.M. 1993, PASP, 105, 247

Peterson, B.M., Wanders, I., Bertram, R., Hunley, J.F., Pogge, R.W., & Wagner, M. 1998a, ApJ, 501, 82

Peterson, B.M., Wanders, I., Horne, K., Collier, S., Alexander, T., & Kaspi, S. 1998b, PASP, 110, 660

Peterson, B.M., et al. 2004, ApJ, 613, 682

Tremaine, S., et al. 2002, ApJ, 574, 740

van Groningen, E., & Wanders, I. 1992, PASP, 104, 700

Watson, L.C. et al. 2008, ApJL, 682, 21

Welsh, W.F. 1999, PASP, 111, 1347

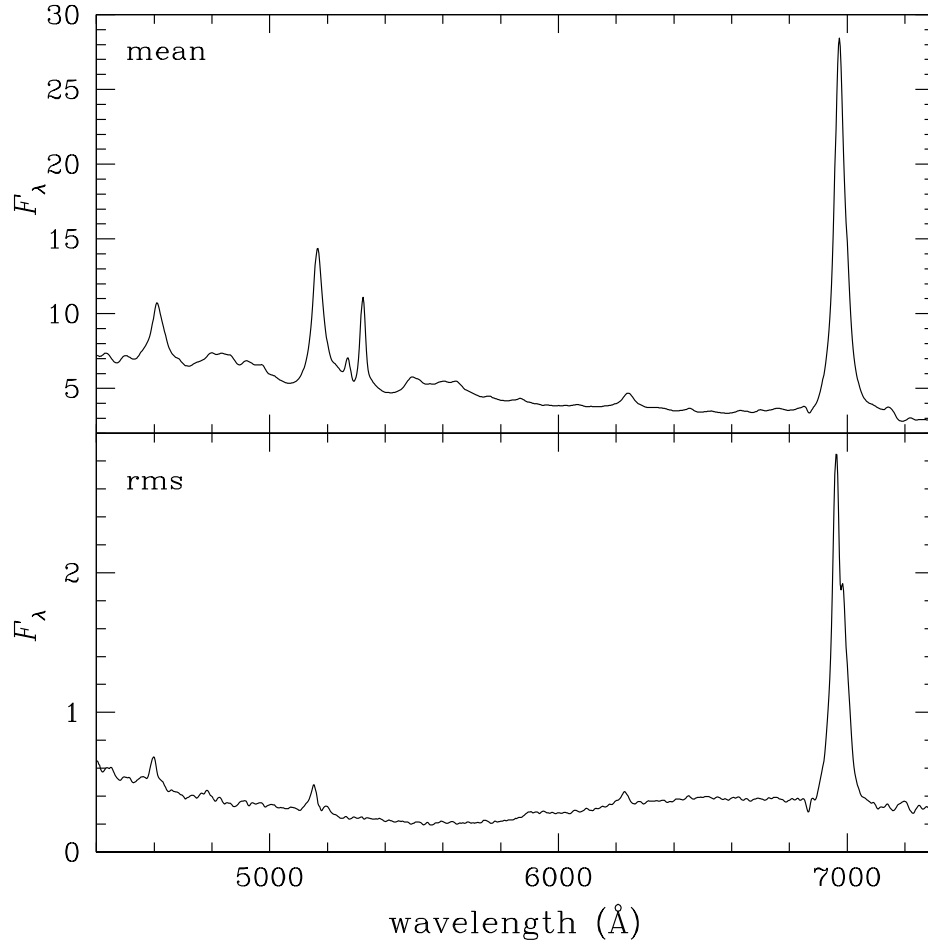


Fig. 1.— The flux-calibrated mean and rms spectra of PG 2130+099 in the observed frame ($z = 0.06298$). The flux density is in units of $10^{-15} \text{ erg s}^{-1} \text{ cm}^{-2} \text{ \AA}^{-1}$.

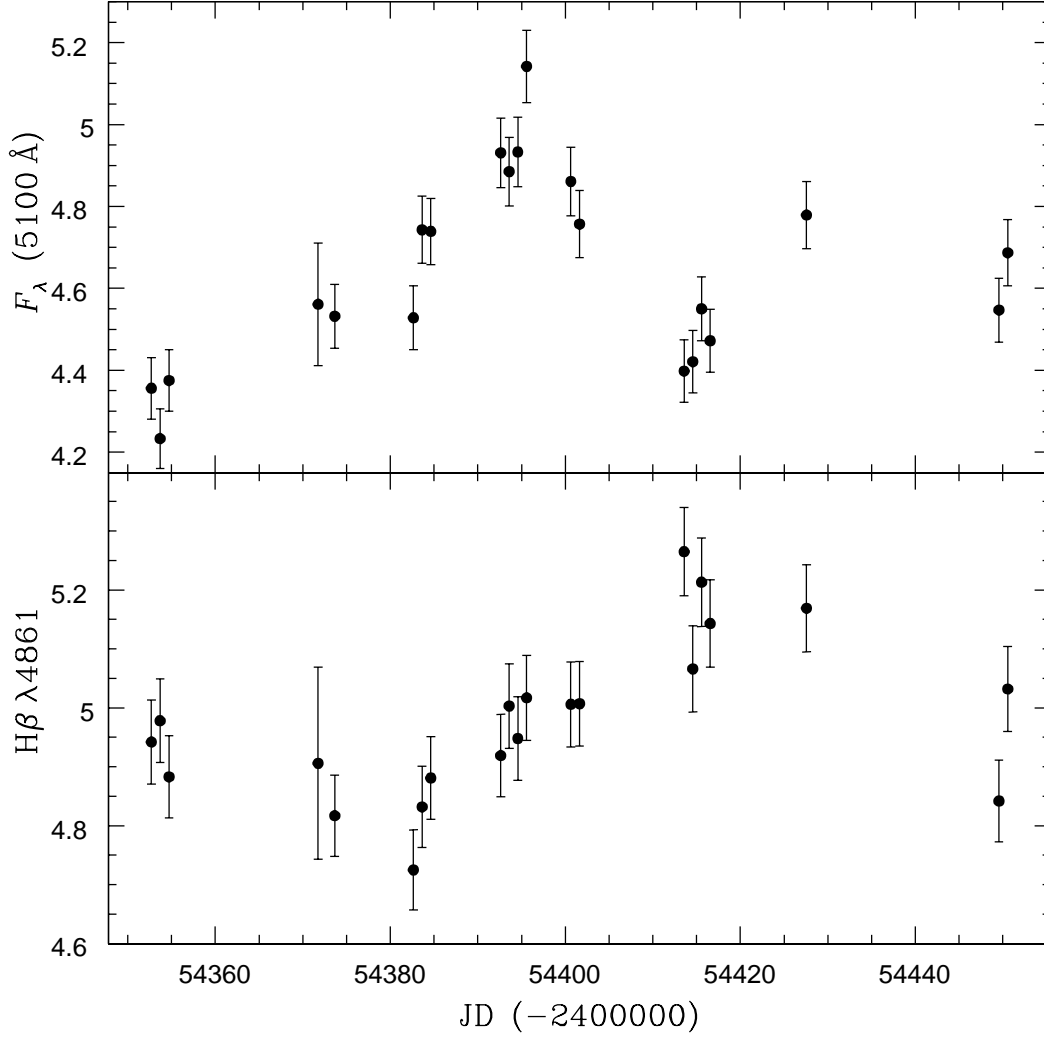


Fig. 2.— Continuum (upper panel) and H β (lower panel) light curves that were used in the time series analysis. Continuum flux densities are in units of $10^{-15} \text{ erg s}^{-1} \text{ cm}^{-2} \text{ \AA}^{-1}$. Emission-line flux densities are in units of $10^{-13} \text{ erg s}^{-1} \text{ cm}^{-2}$. All fluxes are in the observed frame.

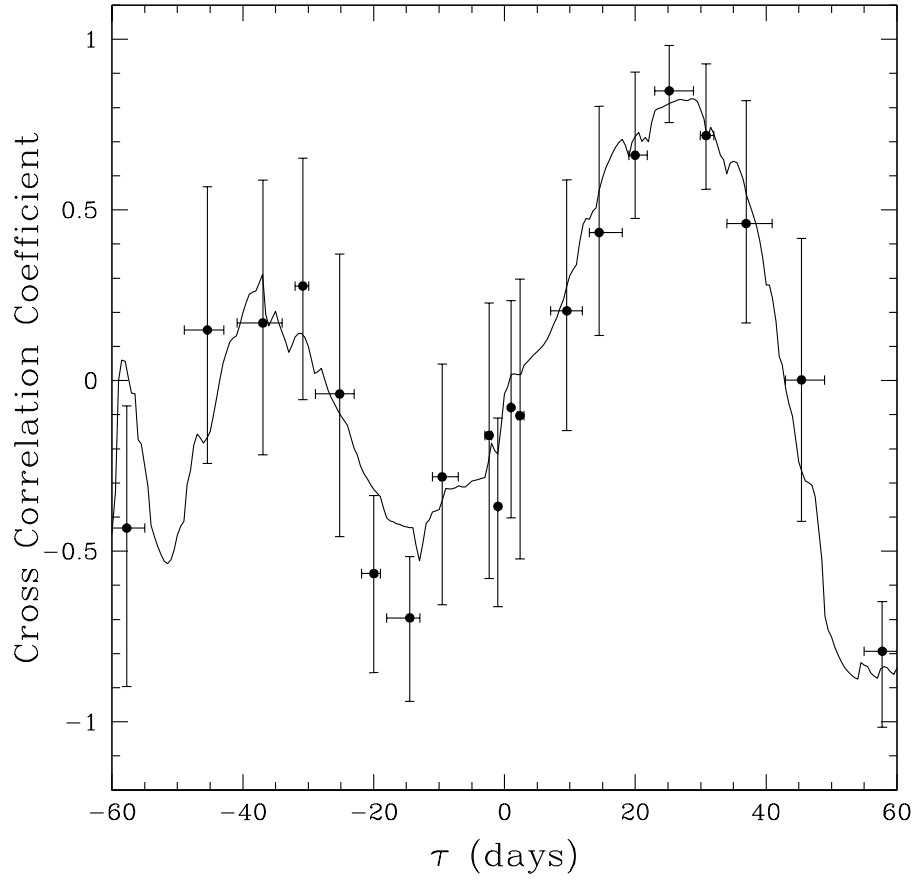


Fig. 3.— The CCF (solid line) and ZDCF (filled circles) from the time series analysis of our recent observations of PG 2130+099.

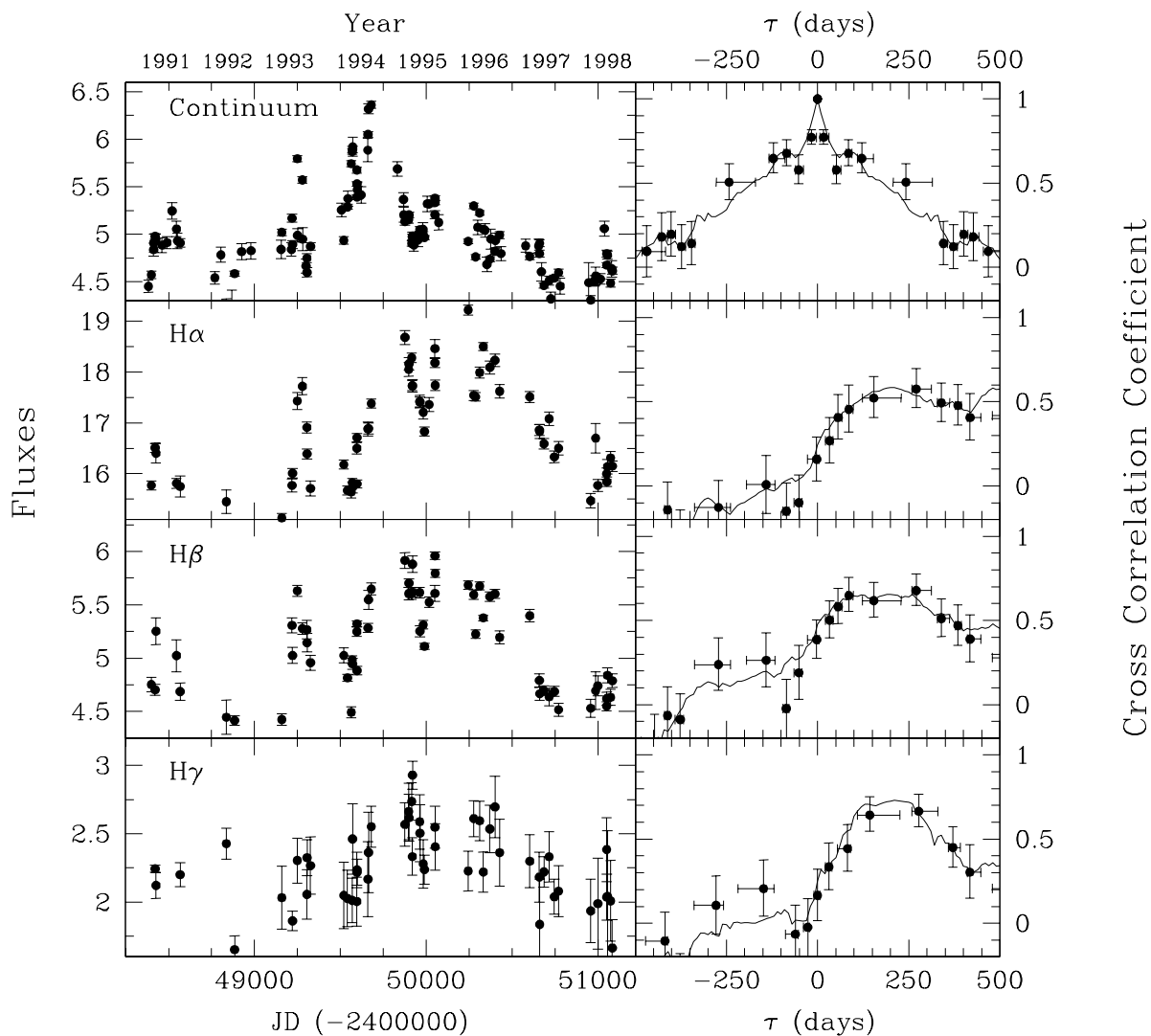


Fig. 4.— The left column shows the light curves of PG 2130+099 from Kaspi et al. (2000). The 5100 Å continuum light curve is shown in the top left panel and the H α , H β , and H γ light curves are displayed below. The right column shows the CCF and corresponding ZDCF for each spectral feature, with the top right panel showing the auto-correlation function (ACF) of the continuum. The continuum flux density is given in units of 10^{-15} erg s $^{-1}$ cm $^{-2}$ Å $^{-1}$ and the H β flux density is in units of 10^{-13} erg s $^{-1}$ cm $^{-2}$.

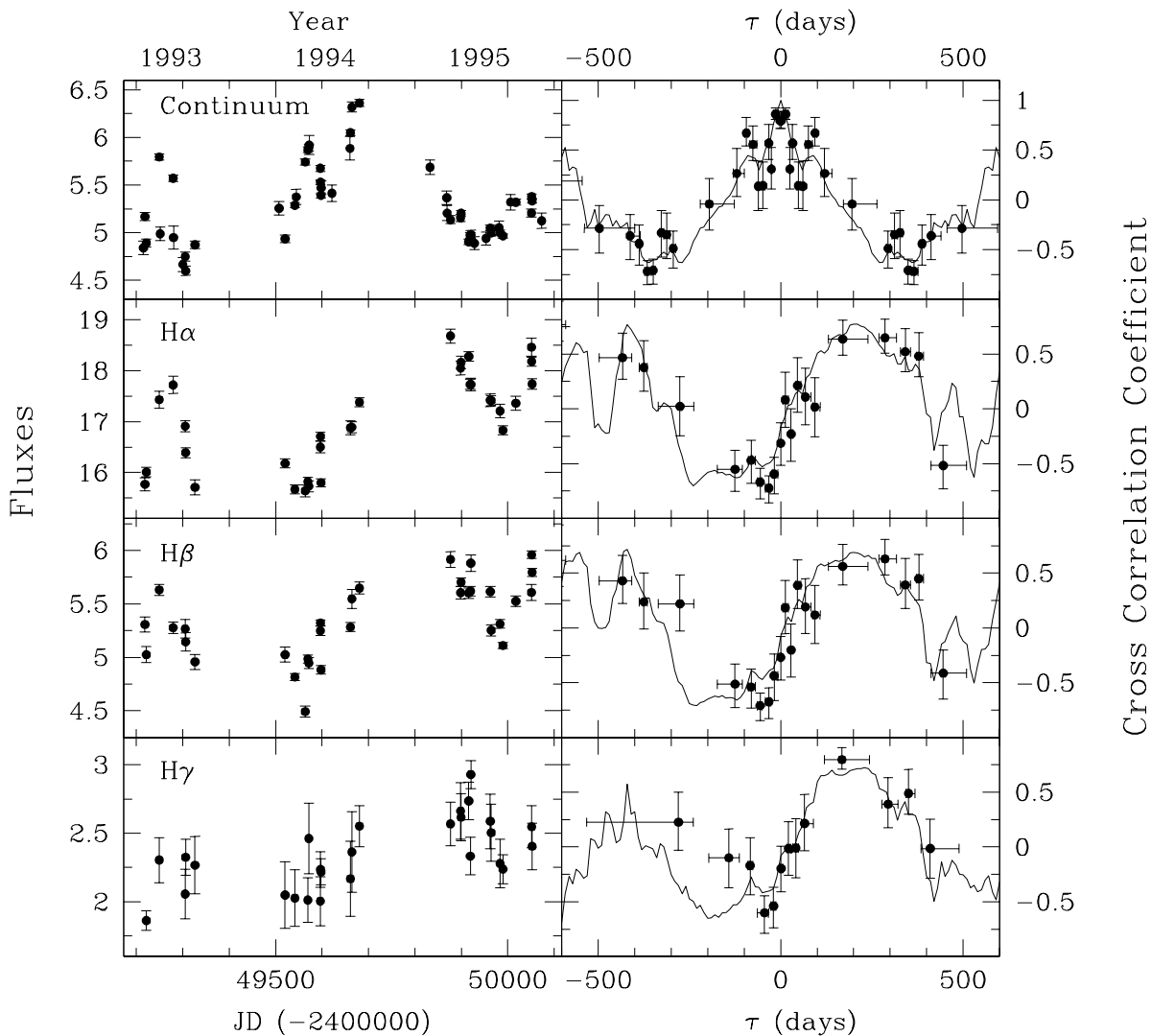


Fig. 5.— Light curves and cross correlation functions for different spectral features of the Kaspi et al. (2000) data. The left column shows a small section of the light curve for each spectral feature. The right column panels show the CCF (solid line) and ZDCF (filled circles) for each feature. The top right panel shows the ACF of the continuum, and the other three panels below show the correlation functions resulting from correlation of each respective emission line with the continuum light curve. The fluxes are given in the same units as in Figure 4.

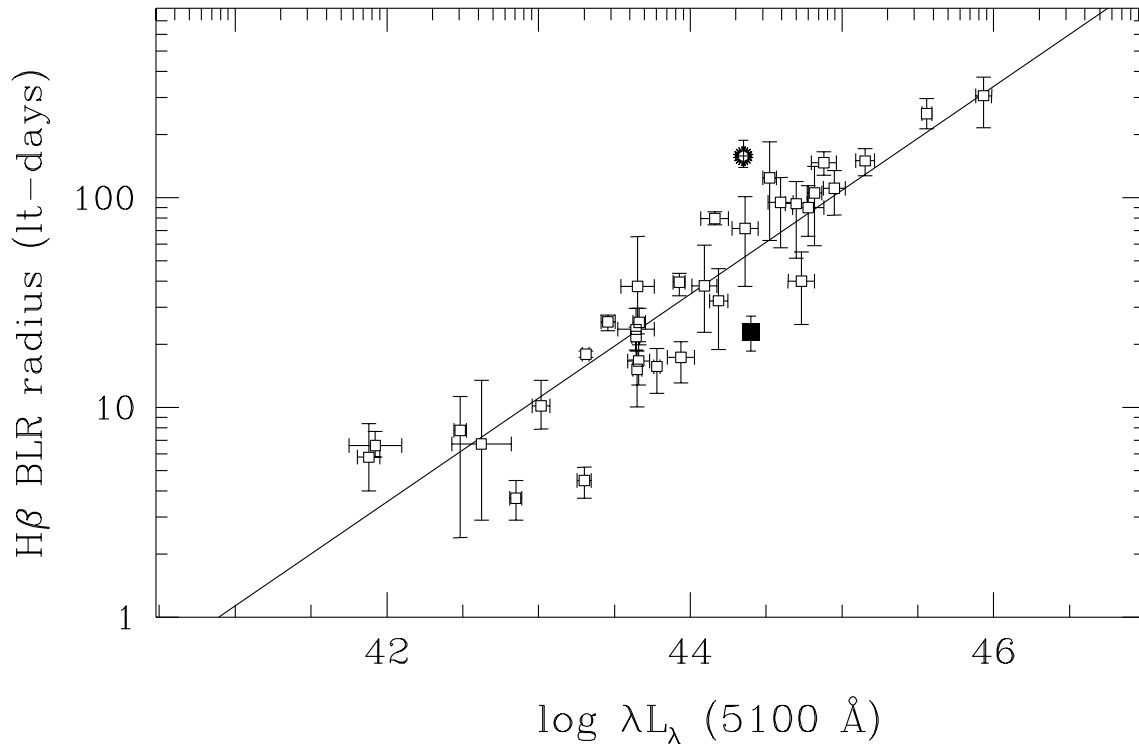


Fig. 6.— The position of PG 2130+099 on the most recent $R_{\text{BLR}}-L$ relationship from Bentz et al. (2008), denoted by the solid line. The starred circle represents the position of PG 2130+099 with a lag of 158.1 days, as given by Peterson et al. (2004). The filled square represents the measurement of 22.9 days from our recent dataset. The open squares represent other objects from Bentz et al.

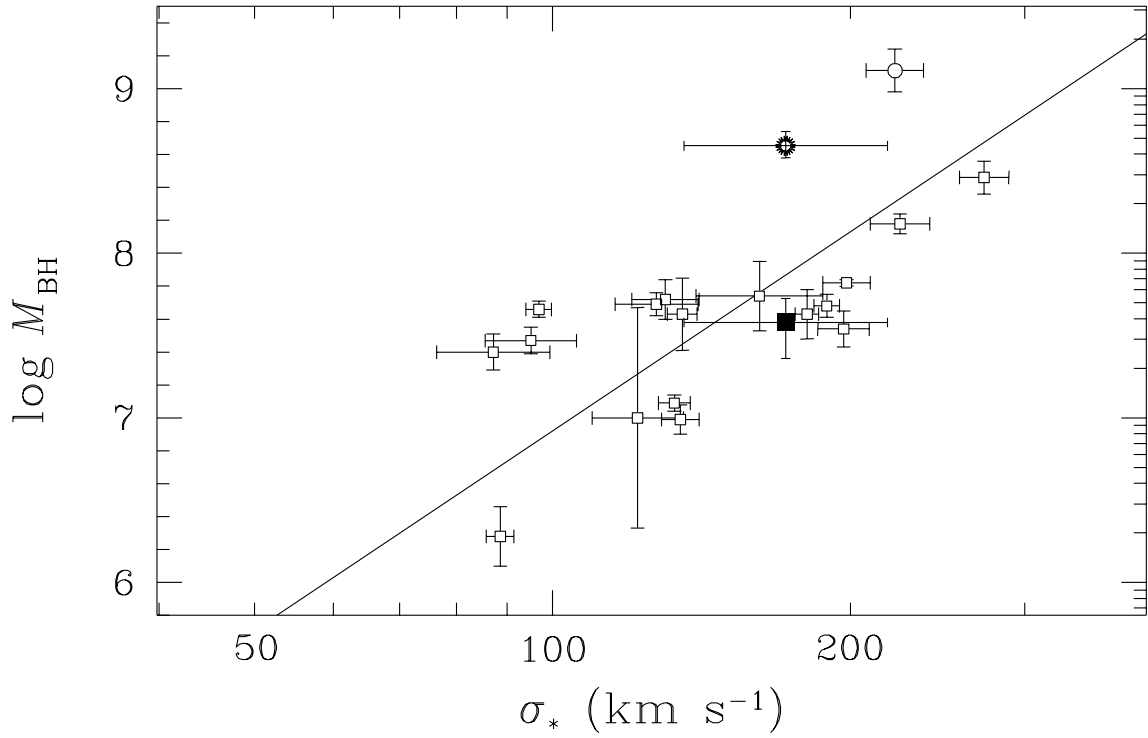


Fig. 7.— The position of PG 2130+099 on the $M_{\text{BH}}-\sigma_*$ relationship (from Tremaine et al. 2002), denoted by the solid line. The open squares show data points based on Onken et al. (2004) and Nelson et al. (2004) and the open circle is PG 1426+015 from Watson et al. (2008). The starred circle and filled square represent the position of PG 2130+099 using the same data sets as in Figure 6.

Table 1. Continuum and H β Fluxes for PG 2130+099

JD (-2400000)	F_λ (5100 Å) (10^{-15} erg s $^{-1}$ cm $^{-2}$ Å $^{-1}$)	H β λ 4861 (10^{-13} erg s $^{-1}$ cm $^{-2}$)
54352.70	4.36 \pm 0.08	4.94 \pm 0.07
54353.70	4.23 \pm 0.07	4.98 \pm 0.07
54354.72	4.38 \pm 0.08	4.88 \pm 0.07
54371.76	4.56 \pm 0.15	4.91 \pm 0.16
54373.65	4.53 \pm 0.08	4.82 \pm 0.07
54382.65	4.53 \pm 0.08	4.73 \pm 0.07
54383.63	4.74 \pm 0.08	4.83 \pm 0.07
54384.64	4.74 \pm 0.08	4.88 \pm 0.07
54392.62	4.93 \pm 0.09	4.92 \pm 0.07
54393.59	4.89 \pm 0.08	5.00 \pm 0.07
54394.57	4.93 \pm 0.08	4.95 \pm 0.07
54395.59	5.14 \pm 0.09	5.02 \pm 0.07
54400.63	4.86 \pm 0.08	5.01 \pm 0.07
54401.63	4.76 \pm 0.08	5.01 \pm 0.07
54413.57	4.40 \pm 0.08	5.27 \pm 0.08
54414.58	4.42 \pm 0.08	5.07 \pm 0.07
54415.57	4.55 \pm 0.08	5.21 \pm 0.08
54416.56	4.47 \pm 0.08	5.14 \pm 0.07
54427.57	4.78 \pm 0.08	5.17 \pm 0.07
54449.56	4.55 \pm 0.08	4.84 \pm 0.07
54450.57	4.69 \pm 0.08	5.03 \pm 0.07

Table 2. Light Curve Statistics

Time Series	Sampling Interval (days)			Mean Flux ¹	Mean Fractional Error	F_{var}	R_{max}
	N	$\langle T \rangle$	T_{median}	(5)	(6)	(7)	(8)
(1)	(2)	(3)	(4)	(5)	(6)	(7)	(8)
5100 Å	21	4.9	1.0	4.64 ± 0.23	0.018	0.047	1.22 ± 0.03
H β	21	4.9	1.0	4.98 ± 0.14	0.015	0.023	1.14 ± 0.02

¹Continuum and emission-line fluxes are given in the same units as Table 1.

Table 3. Reverberation Results

Parameter	Value
(1)	(2)
$\tau_{\text{cent}}^{\text{a}}$	$22.9^{+4.7}_{-4.6}$ days
$\tau_{\text{peak}}^{\text{a}}$	$22.2^{+5.6}_{-5.2}$ days
σ_{line} (mean)	1807 ± 4 km s ⁻¹
FWHM (mean)	2807 ± 4 km s ⁻¹
σ_{line} (rms)	1246 ± 222 km s ⁻¹
FWHM (rms)	2063 ± 720 km s ⁻¹
M_{BH}	$(3.8 \pm 1.5) \times 10^7 M_{\odot}$

^aValues are given in the rest frame of the object.

Table 4. Host Galaxy Flux Removal Parameters

Parameter (1)	Value (2)
Position angle of slit	0.0°
Aperture size	3".0 × 7".0
$F_{\text{galaxy}} (5100 \text{ \AA})^a$	$(0.405 \pm 0.037) \times 10^{-15} \text{ erg s}^{-1} \text{ cm}^{-2} \text{ \AA}^{-1}$
$\log \lambda L_{\lambda}(5100 \text{ \AA})^b$	(44.40 ± 0.02)

^aGalaxy flux is in the observed frame, from Bentz et al. (2008).

^b5100 Å rest-frame luminosity in erg s^{-1} , with host galaxy subtracted and corrected for extinction, following Bentz et al. (2006; 2008).

Table 5. Reverberation Results From Kaspi et al. Dataset

Data Subset	Spectral Feature	τ_{cent} (days)	τ_{peak} (days)
Entire Data Set	H α	215.2 $^{+32.1}_{-27.8}$	217.4 $^{+20.0}_{-20.0}$
Entire Data Set	H β	168.2 $^{+36.7}_{-21.4}$	177.4 $^{+60.0}_{-100.0}$
Entire Data Set	H γ	197.6 $^{+37.9}_{-28.5}$	208.3 $^{+40.0}_{-80.0}$
1993-1995	H α	199.1 $^{+4.8}_{-0.7}$	203.0 $^{+10.0}_{-10.0}$
1993-1995	H β	203.5 $^{+5.2}_{-17.4}$	202.9 $^{+0.0}_{-10.0}$
1993-1995	H γ	195.6 $^{+35.1}_{-27.6}$	219.5 $^{+21.0}_{-93.0}$
1993	H α	15.6 $^{+0.6}_{-1.4}$	19.1 $^{+0.0}_{-3.0}$
1993	H β	12.2 $^{+1.5}_{-2.5}$	13.1 $^{+3.0}_{-2.0}$
1994	H α	15.2 $^{+0.9}_{-1.6}$	16.0 $^{+0.0}_{-0.0}$
1994	H β	13.7 $^{+1.8}_{-0.8}$	16.0 $^{+0.0}_{-1.0}$
1994	H γ	10.0 $^{+5.3}_{-3.4}$	12.0 $^{+51.0}_{-9.0}$
1995	H α	36.6 $^{+4.7}_{-3.3}$	44.0 $^{+0.0}_{-10.0}$
1995	H β	46.5 $^{+4.0}_{-2.9}$	44.0 $^{+8.0}_{-0.0}$
1995	H γ	67.4 $^{+7.7}_{-8.5}$	67.0 $^{+7.7}_{-8.5}$